Inorganic Chemistry

ARTICLE

pubs.acs.org/IC

Incorporating Peptides in the Outer-Coordination Sphere of Bioinspired Electrocatalysts for Hydrogen Production

Avijita Jain, Sheri Lense, John C. Linehan, Simone Raugei, Herman Cho, Daniel L. DuBois, and Wendy J. Shaw*

Chemical and Materials Sciences Division, Pacific Northwest National Laboratory, Richland, Washington 99354, United States

Supporting Information

ABSTRACT: Four new cyclic 1,5-diaza-3,7-diphosphacyclooctane ligands have been prepared and used to synthesize $[Ni(P^{Ph}_2N^{R}_2)_2]^{2+}$ complexes in which R is a mono- or dipeptide. These complexes represent a first step in the development of an outer-coordination sphere for this class of complexes that can mimic the outer-coordination sphere of the active sites of hydrogenase enzymes. Importantly, these complexes retain the electrocatalytic activity of the parent $[Ni(P^{Ph}_2N^{Ph}_2)_2]^{2+}$ complex in an acetonitrile solution with turnover frequencies for hydrogen production ranging from 14 to 25 s^{-1} in the presence of *p*-cyanoanilinium trifluoromethanesulfonate and from 135 to 1000 s^{-1} in the presence of protonated dimethylformamide, with moderately low overpotentials, ~0.3 V. The addition of small amounts of water results in rate increases of 2−7 times. Unlike the parent complex, these complexes demonstrate dynamic structural transformations in solution. These results establish a building block from which larger peptide scaffolding can be added to allow the $[Ni(P^{R}_2N^{R'}_2)_2]^{2+}$ molecular catalytic core to begin to mimic the multifunctional outer-coordination sphere of enzymes.

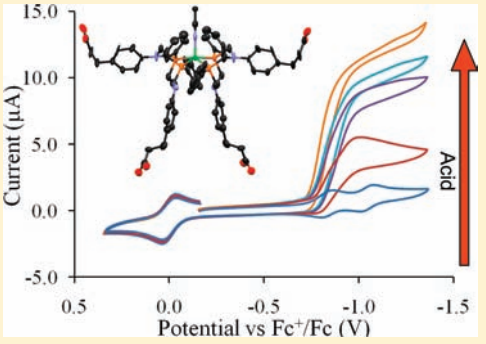

INTRODUCTION

The production of hydrogen from renewable energy sources such as solar or wind will require electrocatalysts for proton reduction. Similarly, the efficient utilization of dihydrogen in fuel cells requires highly active electrocatalysts for the reverse reaction, hydrogen oxidation. While platinum is currently the catalyst of choice for these reactions, naturally occurring hydrogenase enzymes efficiently and rapidly produce and oxidize hydrogen without using expensive metal catalysts.[1−5] While utilizing hydrogenase enzymes directly in fuel cells may have technological challenges, learning from and implementing some of the features of these enzymes can assist in the design of small-molecule catalysts.

Though hydrogenases have been extensively studied, the mechanism by which they achieve fast catalytic rates and very low overpotentials for hydrogen production is not fully understood.[1] The solving of several crystal structures in the mid-1990s revealed bimetallic active sites consisting of abundant metals, either nickel and iron or iron and iron.[4,6,7] Many structural mimics of the bimetallic iron [FeFe] (**1**) or heterobimetallic nickel−iron [NiFe] complexes[1,7] have been prepared but have been found to catalyze dihydrogen production and oxidation much more slowly than hydrogenase or with higher overpotentials.[8] The pendant base in [FeFe] hydrogenases has been suggested to serve as a relay for the transfer of protons from the metal to the proton conduction channels.[3,7] Using this design principle, synthetic functional analogues of hydrogenases were prepared for the electrochemical oxidation and production of dihydrogen.[9−18] This work demonstrated that the functional hydrogenase mimics with a properly positioned pendant amine, or proton relay, can approach the rates of [NiFe] hydrogenase enzymes for dihydrogen production (350 and 750 s^{-1}, respectively).[2,15] In particular, nickel catalysts with 1,5-diaza-3,7-diphosphacyclooctane ligands ($P^{R}_2N^{R'}_2$; **2**) with the general formula $[Ni(P^{R}_2N^{R'}_2)_2]^{2+}$ exhibit rates for dihydrogen production and oxidation that are at least 2−3 orders of magnitude larger than those for analogous complexes without the positioned relay.[11,12,14−16,19,20]

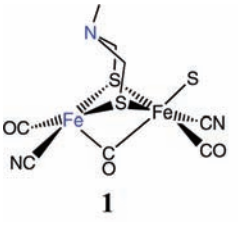

1

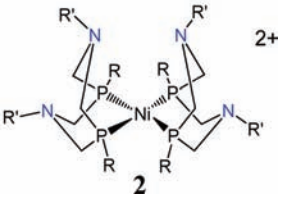

2

Although a number of nickel-based electrocatalysts have been reported, these synthetic catalysts still fall short of the rate of the fastest hydrogenases, [FeFe] (10 000 s^{-1}).[2,21] The significant

Received: December 30, 2010
Published: April 01, 2011

rate enhancement due to the second coordination sphere in small-molecule catalysts, as well as the structural features of the enzyme, suggests that the outer-coordination sphere may also contribute significantly to catalysis at the active site. As a starting point to mimic the function of the protein scaffold, we have incorporated small peptides into $[Ni(P_2^RN_2^{R'})_2]^{2+}$ electrocatalysts. In this work, we report the synthesis of new $P^R{}_2N^{R'}{}_2$ ligands containing unnatural amino acids and dipeptides on the central nitrogen atom. These small biologically based ligands serve as a starting point for the preparation of $[Ni(P^{Ph}{}_2N^R{}_2)_2]^{2+}$ complexes with peptide functional units in the outer-coordination sphere. They also provide a comparison of the catalytic activities of these complexes relative to the parent $[Ni(P^{Ph}{}_2N^{Ph}{}_2)_2]^{2+}$ catalyst, before incorporating larger peptides into the outer-coordination sphere.

MATERIALS AND METHODS

General Procedures. Solution-state ^1H and ^{31}P NMR spectra were recorded on a Varian Inova or VnmrS spectrometer (500 MHz ^1H frequency). All ^1H chemical shifts were internally calibrated to the monoprotic solvent impurity. All $^{31}P\{^1H\}$ chemical shifts were externally referenced to phosphoric acid. Solid-state $^{31}P\{^1H\}$ NMR spectra were run on a Chemagnetics console using a single pulse excitation and spinning at 11.5 kHz. Elemental analyses were done by Atlantic Microlab, Norcross, GA, with V_2O_5 as a combustion catalyst. Electrospray ionization (ESI) and chemical ionization mass spectrometry (MS) spectra were collected at the Indiana University Mass Spectrometry Facility on a Waters/Micromass LCT Classic using anhydrous solvents and inert-atmosphere techniques.

Synthesis and Materials. Acetonitrile was purchased from Alfa Aesar and ethyl ether from Honeywell Burdick & Jackson, and they were dried using an activated alumina column. 3-(4-Aminophenyl)propionic acid and 3-(4-aminophenyl)propionic ethyl ester were purchased from Sigma Aldrich. All reactions were performed using standard Schlenk techniques under a dinitrogen atmosphere or in a glovebox unless otherwise noted. Dicyclohexyl carbodiimide (DCC) and (dimethylamino)-pyridine (DMAP) were purchased from Sigma Aldrich. $PhP(CH_2OH)_2$ was prepared by reacting 1 equiv of $PhPH_2$ with 2 equiv of *p*-formaldehyde.[19]

*$P_2^{Ph}N_2^{AA}$ (**3a**; AA = Amino Acid).* **3a** was synthesized following a previously published preparation.[22] A solution of 3-(4-aminophenyl)-propionic acid (0.49 g, 3.0 mmol) in ethanol was added to a solution of $PhP(CH_2OH)_2$ (0.51 g, 3.0 mmol) in ethanol (30 mL) in a glovebox, and the mixture was heated to 65 °C for 16 h to form a white precipitate. The solution was cooled to room temperature, and the product was filtered using 20 mL of ethanol to rinse it from the flask and 20 mL of ethanol to wash the solid. The yield obtained was 0.76 g, 0.13 mmol, 85%. The resulting product was not soluble in common organic solvents but was soluble in basic water (pH 10). $^{31}P\{^1H\}$ NMR: δ −50.0. ^1H NMR (basic D_2O): δ 7.40, 7.34, 6.87, 6.39 (m, 18H, Ar−*H*), 3.96 (d, 4H, PCH_2N), 4.06 (d, 4H, PCH_2N), 2.52 (t, 4H, CH_2COO), 2.16 (t, 4H, $PhCH_2$). Elem anal. Calcd for $C_{34}H_{36}N_2O_4P_2$: C, 68.22; H, 6.06; N, 4.68. Found: C, 68.29; H, 6.14; N, 4.73. ESI MS: *m/z* 621 $\{(P_2^{Ph}N_2^{APPA})_2] + Na\}^+$.

*$P_2^{Ph}N_2^{AAE}$ (**3b**; AAE = Amino Acid Ester).* This ligand was prepared in a manner analogous to that of **3a** using $PhP(CH_2OH)_2$ and 3-(4-aminophenyl)propionic ester (0.582 g, 3 mmol) to form a pale-yellow solid. Yield: 0.85 g, 1.30 mmol, 87%. $^{31}P\{^1H\}$ NMR (CD_2Cl_2): δ −50.5 (s). ^1H NMR (CD_2Cl_2): δ 6.66, 7.04, 7.48, 7.62 (M, 18H, Ar−*H*), 1.21 (t, 6H, CH_3), 4.07 (m, 4H, PCH_2N and 4H, CH_2COO), 4.41 (q, 4H, $COOCH_2$), 2.79 (t, 4H, CH_2COO), 2.51 (t, 4H, $PhCH_2$). Elem anal. Calcd for $C_{38}H_{44}N_2O_4P_2$: C, 69.71; H, 6.77; N, 4.28. Found: C, 69.60; H, 6.80; N, 4.37. ESI MS: *m/z* 655 $\{(P_2^{Ph}N_2^{AA})_2] + H\}^+$.

*$P_2^{Ph}N_2^{DPE}$ (**3c**; DPE = Dipeptide Ester).* To a solution of glycine ethyl ester·H_3PO_4 (0.168 g, 0.830 mmol) in tetrahydrofuran (25 mL) were added **3a** (0.244 g, 0.41 mmol), DMAP (0.109 g, 0.896 mmol), and DCC (0.185 g, 0.896 mmol). The reaction mixture was stirred at room temperature for 19 h. The suspended impurities were removed by filtration through Celite. The solvent was removed under vacuum, and the solid was collected. Yield: 0.282 g, 0.74 mmol, 82%. $^{31}P\{^1H\}$ NMR (CD_2Cl_2): δ −50.5 (s). ^1H NMR (CD_2Cl_2): δ 6.68, 7.05, 7.46, 7.63 (m, 18H, Ar−*H*), 8.09 (s, 2H, N*H*), 4.38 (m, 4H, NCH_2COO), 4.14 (q, 4H, $COOCH_2$), 4.07 (d, 4H, PCH_2N), 3.96 (d, 4H, PCH_2N), 2.80 (t, 4H, CH_2COO), 2.44 (t, 4H, $PhCH_2$), 1.29 (t, 6H, CH_3).

*$[Ni(P_2^{Ph}N_2^{AA})_2](BF_4)_2$ (**4a**).* Solid **3a** (0.957 g, 1.60 mmol) and $[Ni(CH_3CN)_6](BF_4)_2$ (0.4 g, 0.8 mmol) were stirred for 24 h in acetonitrile (20 mL) to give a red solution. The solution was filtered using a medium frit to remove small amounts of suspended impurities. The solvent was removed under vacuum, and the residue was dissolved in 5 mL of acetonitrile. The product was then flash-precipitated by addition to 60 mL of stirring diethyl ether. Yield: 1.05 g, 0.74 mmol, 92%. ^1H NMR (CD_3CN): δ 7.41, 7.29, 7.17 (m, 36H, Ar−*H*), 3.90 (d, 8H, PCH_2N), 4.21 (d, 8H, PCH_2N), 2.90 (t, 8H, CH_2COO), 2.63 (t, 8H, $PhCH_2$), 9.04 (s, 4H, COO*H*). $^{31}P\{^1H\}$ NMR (CD_3CN): δ 5.33 (s). Elem anal. Calcd for $C_{68}H_{72}N_4O_8P_4NiB_2F_8$: C, 57.17; H, 5.08; N, 3.92. Found: C, 55.55; H, 4.98; N, 4.08. ESI MS (CH_3CN): *m/z* 1341 $\{[Ni(P_2^{Ph}N_2^{DPA})_2](BF_4)\}^+$. A cyclic voltammogram recorded in $^nBu_4N^+OTf^-$/benzonitrile consisted of two reversible reduction waves at −0.82 and −1.02 V corresponding to the $Ni^{II/I}$ and $Ni^{I/0}$ couples.

*$[Ni(P_2^{Ph}N_2^{AAE})_2](BF_4)_2$ (**4b**).* Complex **4b** was prepared in a manner analogous to that of **4a** using **3b** (0.1046 g, 1.6 mmol) and $[Ni(CH_3CN)_6](BF_4)_2$. Yield: 0.700 g, 0.45 mmol, 91%. ^1H NMR (CD_3CN): δ 7.41, 7.27, 7.17 (m, 36H, Ar−*H*), 1.18 (t, 12H, CH_3), 3.90 (d, 8H, PCH_2N), 4.06 (q, 8H, $COOCH_2$), 4.18 (d, 8H, PCH_2N), 2.93 (t, 8H, CH_2COO), 2.63 (t, 8H, $PhCH_2$). $^{31}P\{^1H\}$ NMR (CD_3CN): δ 4.99 (s). Elem anal. Calcd for $C_{76}H_{88}N_4O_8P_4NiB_2F_8$: C, 59.21; H, 5.75; N, 3.63. Found: C, 56.42; H, 5.59; N, 3.86. ESI MS (CH_3CN): *m/z* 1451 $\{[Ni(P_2^{Ph}N_2^{AAE})_2](BF_4)\}^+$. A cyclic voltammogram recorded in $^nBu_4N^+OTf^-$/acetonitrile consisted of two reversible reduction waves at −0.83 and −1.04 V corresponding to the $Ni^{II/I}$ and $Ni^{I/0}$ couples.

*$[Ni(P_2^{Ph}N_2^{DPE})_2](PF_6)_2$ (**4c**).* Solid **3c** (0.100 g, 0.125 mmol) and $[Ni(CH_3CN)_6](PF_6)_2$ (0.036 g, 0.062 mmol) were stirred for 3 days in acetonitrile (20 mL) to give a red solution. The solution was filtered using a medium frit to remove small amounts of suspended impurities. The solvent was removed under vacuum, and the residue was dissolved in 5 mL of acetonitrile. The product was then flash-precipitated by addition to 60 mL of stirring diethyl ether. Yield: 0.093 g, 0.53 mmol, 85%. $^{31}P\{^1H\}$ NMR (CD_3CN): δ 4.04 (s), 21.6 (s), −13.6 (s). ^1H NMR (CD_3CN): δ 6.88, 7.20, 7.94 (m, 36H, Ar−*H*), 8.03 (s, 4H, N*H*), 4.20 (m, 8H, NCH_2COO), 4.15 (d, 8H, PCH_2N), 3.86 (d, 8H, PCH_2N), 3.42 (q, 8H, $COOCH_2$), 2.92 (t, 8H, CH_2COO), 2.63 (t, 8H, $PhCH_2$), 1.29 (t, 6H, CH_3). ESI MS (CH_3CN): *m/z* 1739 $\{[Ni(P_2^{Ph}N_2^{DPE})_2]$-$(PF_6)\}^+$. A cyclic voltammogram recorded in $^nBu_4N^+OTf^-$/acetonitrile consisted of one reversible reduction wave at −0.83 V corresponding to the $Ni^{II/I}$ couple and one quasireversible reduction wave at −1.03 V corresponding to the $Ni^{I/0}$ couple.

*$[Ni(P_2^{Ph}N_2^{DPA})_2](PF_6)_2$ (**4d**; DPA = Dipeptide Acid).* **4d** was synthesized on a polystyrene-based Wang resin (Novabiochem, San Diego, CA), using solid-phase peptide synthesis techniques.[23] The fluorenylmethoxycarbonyl (FMOC) group was removed by stirring a glycine-substituted Wang resin (0.181 g, 0.61 mmol) with 20 mL of 20% piperidine in *N*-methylpyrrolidone (NMP). The solid was rinsed with NMP and CH_2Cl_2 and collected by filtration using a medium frit. Ligand **3a** (0.182 g, 0.305 mmol), DMAP (0.075 g, 0.61 mmol), and DCC (0.125 g, 0.61 mmol) were added to the FMOC-deprotected glycine resin (0.181 g, 0.61 mmol) in 25 mL of dichloromethane.

dx.doi.org/10.1021/ic1025872 |*Inorg. Chem.* 2011, 50, 4073–4085

The solution was stirred at room temperature for 19 h, followed by filtration using a medium frit and collection of the peptidyl resin. The resin was rinsed with 70 mL of dichloromethane to remove unreacted DMAP and DCC. Solid-state $^{31}P\{^1H\}$: δ −40.8 (s), −34.4 (s). The resin obtained was suspended in 30 mL of acetonitrile, and $[Ni(CH_3CN)_6](PF_6)_2$ (0.181 g, 0.305 mmol) was then added. The reaction mixture was stirred at room temperature for 5 days, resulting in a red resin. The light-red solution was filtered using a medium frit, and the red solid was collected. To cleave the complex from the resin, trifluoroacetic acid (4.75 mL), triisopropylsilane (0.125 mL), and water (0.125 mL) were added to the solid and the resulting solution was stirred for 4 h. The resulting reaction mixture was filtered, and the volume of the filtrate was reduced to 1 mL under vacuum. The product was then flash-precipitated by addition of this solution to 60 mL of stirring diethyl ether. Yield: 0.34 g, 0.21 mmol, 68%. Solid-state $^{31}P\{^1H\}$: δ 21.5 (s), −13.4 (s). Solution-state $^{31}P\{^1H\}$ NMR (CD_3CN): δ 4.04 (s), 22.14 (s), −13.7 (s). ^1H NMR (CD_3CN); δ 7.39, 7.26, 7.14 (m, 36H, Ar−*H*), 7.98 (s, 4H, N*H*), 4.24 (d, 8H, PCH_2N), 3.76 (d, 8H, COCH_2N), 3.98 (d, 8H, PCH_2N), 2.90 (t, 8H, CH_2COO), 2.63 (t, 8H, PhCH_2). ESI MS (CH_3CN): *m*/*z* 1627 $\{[Ni(P_2^{Ph}N_2^{DPA})_2](PF_6)\}^+$. Note: Dichloromethane was run through basic alumina before use. If the catalysts were prepared in reagent-grade dichloromethane, a chloride ion was incorporated because of residual HCl, resulting in a small portion of a five-coordinate chloride complex. This complex resulted in asymmetric resonances about the central phosphorus resonance that were distinct from those observed for the dipeptides. A cyclic voltammogram recorded in $^nBu_4N^+OTf^-$/acetonitrile consisted of one reversible reduction wave at −0.84 V corresponding to the $Ni^{II/I}$ couple and one quasi-reversible reduction wave at −1.03 V corresponding to the $Ni^{I/0}$ couple.

Peptide Titration Studies. Metal complex **4b** was titrated with various concentrations of the ethyl ester of the glycylglycine dipeptide to investigate interaction of the amide functionality with the nickel metal center. Stock solutions of complex **4b** (5 mL, 2.8 mM) and the ethyl ester of the glycylglycine dipeptide (5 mL, 28 mM) were made in methanol-*d*. The two solutions were mixed in order to get 1:1, 1:2, and 1:4 dipeptide-to-metal complex ratios. $^{31}P\{^1H\}$ NMR spectra of the solutions were recorded, and all chemical shifts were externally referenced to phosphoric acid.

Electrochemical Studies. All cyclic voltammetry experiments were carried out on a computer-aided CHI 1100 A potentiostat under a dinitrogen atmosphere in 0.2 M $^nBu_4N^+OTf^-$/acetonitrile solutions at a scan rate of 50 mV/s. The electrochemistry of complex **4a** was investigated in benzonitrile. The working electrode used was a glassy carbon disk, and the counter electrode was a glassy carbon rod. A silver wire was used as a pseudoreference electrode. Ferrocene was used as an internal standard, and all potentials are referenced to the ferrocenium/ferrocene couple.

Dependence of the Catalytic Current on the Acid Concentration. Metal complexes were titrated with acetonitrile solutions containing *p*-cyanoanilinium trifluoromethanesulfonate (*p*-cyanoanilinium) or the triflate salt of protonated dimethylformamide ($DMFH^+$) in order to determine the order of the reaction with respect to acid. A total of 1.0 mL of a 0.7 mM solution of each metal complex in acetonitrile containing a 0.2 M electrolyte ($^nBu_4N^+OTf^-$ was used with *p*-cyanoanilinium, and $Et_4N^+BF_4^-$ was used with $DMFH^+$) was made. The solution was syringe-filtered using a 1.6 μm poly(tetrafluoroethylene) syringe filter. The solution was then purged with dinitrogen for 5 min, and the initial voltammogram was measured. The cathodic current (i_p) for the $Ni^{II/I}$ couple was recorded. Aliquots of acid were added via microsyringe in 10−100 μL increments until the catalytic current stopped increasing. The cathodic current (i_p) was corrected for dilution, and the catalytic current (i_c) at −0.94 V was measured. The ratios of i_c/i_p versus the acid concentration were plotted to determine the order with respect to acid. At the end of the experiment, degassed water was added in 5 μL increments until the catalytic current stopped increasing. Each measurement was repeated multiple times for statistical purposes.

Dependence of the Catalytic Current on the Catalyst Concentration. A solution containing 20 mM *p*-cyanoanilinium was prepared in 0.2 M $NEt_4^+OTf^-$/acetonitrile. Aliquots of a 2 mM stock solution of catalyst **4a** containing 20 mM *p*-cyanoanilinium prepared in 0.2 M $NEt_4^+OTf^-$/acetonitrile were added to 1.0 mL of the first solution. The catalytic current i_c was measured at −0.94 V. A plot of the catalytic current versus the catalyst concentration was used to determine the order with respect to the catalyst.

Controlled-Potential Coulometry. A three-necked flask having a total volume of 147 mL was used for bulk electrolysis experiments. A cylinder of reticulated vitreous carbon (working electrode) was introduced in a flask via a rubber septum. The reference and counter electrodes were silver and nickel−chromium wires, respectively, placed in 7 mm glass tubes terminating in Vycor fritted disks and filled with an electrolyte solution (0.2 M Et_4NBF_4 in acetonitrile). The cell was purged with dinitrogen for 20 min prior to the experiment. A 25 mL solution of metal complex **4c** (1 mM) and a 2 mL solution of $DMFH^+$ (50 mM) were added to the flask. Controlled-potential coulometry was performed at −0.95 V versus the ferrocenium/ferrocene couple. After 17.6 C of charge was passed, a 300 μL sample of the headspace gas was removed via a gastight syringe and analyzed by gas chromatography. From this data, it was found that 4.6 mol of dihydrogen were produced per 1 mol of catalyst and a current efficiency of 93% was calculated for dihydrogen production, similar to other catalysts of this type.[15] An aliquot of the catalytic solution was analyzed by ^{31}P NMR spectroscopy, and 80% of the original catalyst remained.

X-ray Crystallography. Crystals of **4a** were grown by the slow diffusion of ether into a MeCN solution of **4a** at room temperature. A 0.05 × 0.05 × 0.16 cm^3 orange, block-shaped crystal was selected, mounted on a MiTeGen MicroMounts pin using Paratone-N oil, and cooled to the data collection temperature of 100(2) K. Data were collected on a Brüker-AXS Kappa Apex II CCD diffractometer with 0.710 73 Å Mo Kα radiation. Data were measured using ω and φ scans of 0.5°/frame for 35 s. The final resolution was 0.72 Å. Cell parameters were retrieved using Brüker *APEXII* software,[24] raw data were integrated using *SAINTPlus*,[25] and absorption correction was applied using *SADABS*.[26] The structure was solved using the Patterson method and refined by a least-squares method on F^2 using the *SHELXTL* program package.[27] The structure was solved in the space group *Pnn*2 (No. 34) by analysis of systematic absences and intensity statistics.

The $[Ni(P_2^{Ph}N_2^{AA})_2(CH_3CN)]^{2+}$ cation is centered on a special position with the halves of the cation related by symmetry. All atoms in the main residue that were not part of the disorder modeling were refined anisotropically. There was considerable disorder among the nitrogen-bound phenyl groups. The disordered phenyl group composed of atoms C15−C20 was modeled by assigning two different orientations to the phenyl ring about the axis through the C15 and C18 atoms (C16, C17, C19, C20 and C16A, C17A, C19A, C20A, each having 50% occupancy). In order to prevent abnormally short and long bond distances, atoms C15, C16, C517, C18, C7A, and C8A were constrained to a regular hexagon, d = 1.39 Å, and the bond distances for C15−C16A, C17A−C18, C15−C20A, and C19A−C20A were restrained to the same distances. Similarly, the disordered phenyl group composed of atoms C26−C31 was modeled by assigning two different orientations to the phenyl ring about the axis through atoms C26 and C29 (C27, C28, C30, C31 and C27A, C28A, C30A, C31A). The disordered atoms could not be refined anisotropically and were thus refined isotropically. A solvent ether molecule, occupancy 50%, is also present in the structure. The bond distances of the solvent molecule were restrained to >1.4 Å to prevent abnormally short bond distances. Crystal data for $[Ni(P_2^{Ph}N_2^{AA})_2(CH_3CN)](BF_4)_2$ are shown in Table S1 in the Supporting Information.

dx.doi.org/10.1021/ic1025872 |*Inorg. Chem.* 2011, 50, 4073–4085

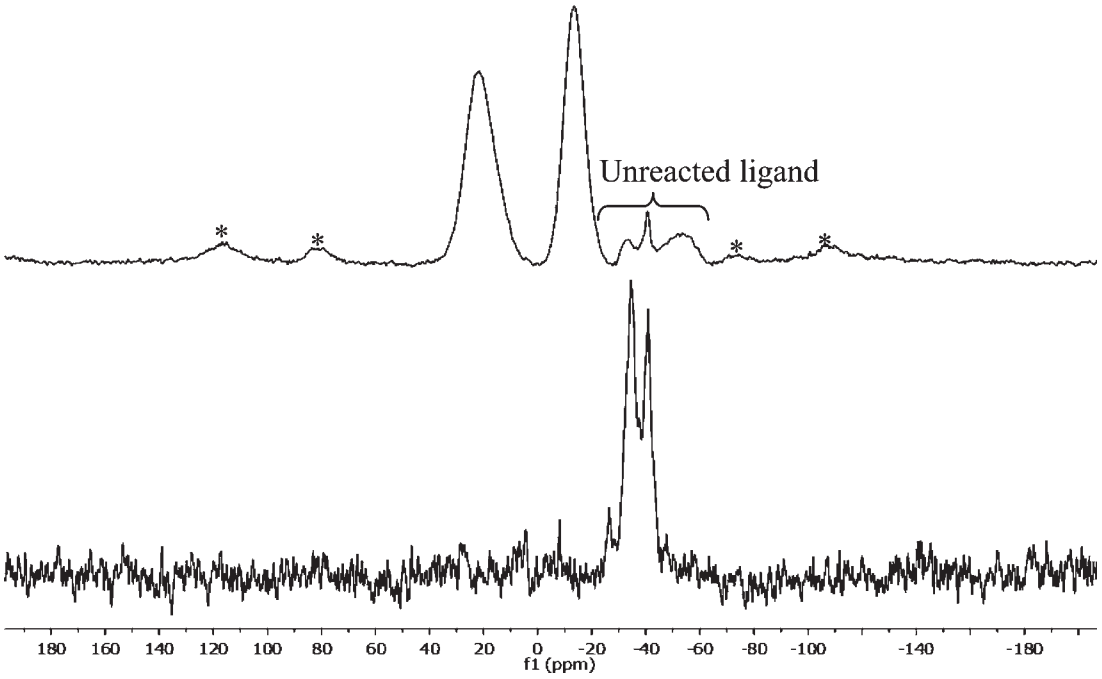

Figure 1. Solid-state ^{31}P NMR of ligand **3d** (bottom) and metal complex **4d** (top) before cleavage from the resin. Spinning side bands are indicated by asterisks.

Computational Methods. A gas-phase model for the complex was built starting from the crystal structure of the $[Ni(P^{Ph}{}_2N^{Ph}{}_2)_2]^{2+}$ complex.[15] The structure was relaxed using the conjugated gradient scheme and the semiempirical PM6 force evaluation method,[28] which has been proven to reproduce with good accuracy geometries and, in some cases, energies of metal complexes when compared to more demanding ab initio methods (see, for instance, refs 29 and 30). All of the calculations have been performed using the CP2K code.[31]

RESULTS

Synthesis and Spectroscopic Studies. One of the major objectives in this work was to develop a synthetic approach that would permit the incorporation of the catalytically active $[Ni(P^{Ph}{}_2N^{Ph}{}_2)_2]^{2+}$ core into a polypeptide matrix. To achieve this objective, we used the unnatural amino acid 3-(4-aminophenyl)propionic acid to prepare the cyclic diphosphine ligand **3a**, as shown in reaction (1) for R = H. The presence of the carboxylic acid group allows the attachment of additional amino acids

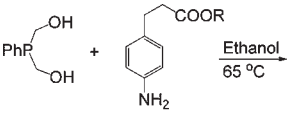

3a R = H
3b R = Et (1)

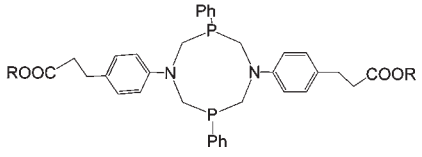

or small peptides, while the presence of the phenyl substituent on nitrogen should ensure the same electronic environment as the $P^{Ph}{}_2N^{Ph}{}_2$ ligand used in the $[Ni(P^{Ph}{}_2N^{Ph}{}_2)_2]^{2+}$ complex, a highly active electrocatalyst for dihydrogen production.[15,20] Ligand **3a** is not soluble in common organic solvents but is soluble in basic D_2O solutions. A $^{31}P\{^1H\}$ NMR spectrum recorded in this solvent exhibited a single resonance as expected, and the ^{1}H NMR and mass spectral data are consistent with the proposed structure. The corresponding ester, R = Et, was also prepared for comparison (**3b**). This ligand is soluble in common organic solvents and avoids the more reactive carboxylic acid groups that might influence the chemistry of the target nickel complexes. The $^{31}P\{^1H\}$ and ^{1}H NMR spectra, elemental analyses, and mass spectrometery data are all consistent with the assigned structure of ligand **3b**.

A second amino acid can be incorporated into the outer-coordination sphere of the ligand **3a** by reaction with glycine ethyl ester, as shown in reaction (2), to form the glycine ethyl ester derivative **3c**. Glycine was chosen as the amino acid because its lack of functional groups provides a simple platform to begin our studies. $^{31}P\{^1H\}$ and ^{1}H NMR spectra and mass spectrometry data are all consistent with the assigned structure of **3c**. Similar attempts to prepare the acid from $P_2{}^{Ph}N_2{}^{DPA}$, using glycine instead of its ethyl ester, resulted in a red reaction mixture, and the $^{31}P\{^1H\}$ and ^{1}H NMR spectra of the reaction mixtures indicated a complex distribution of products.

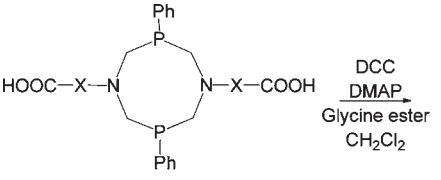

(2)

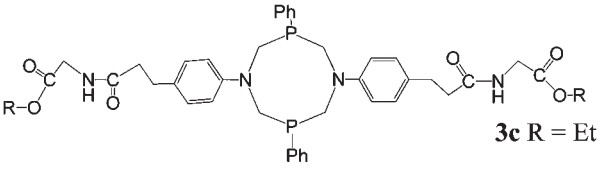

3c R = Et

To overcome the presence for what were apparently unwanted side reactions and to determine if solid-phase synthesis methods

dx.doi.org/10.1021/ic1025872 |*Inorg. Chem.* 2011, 50, 4073–4085

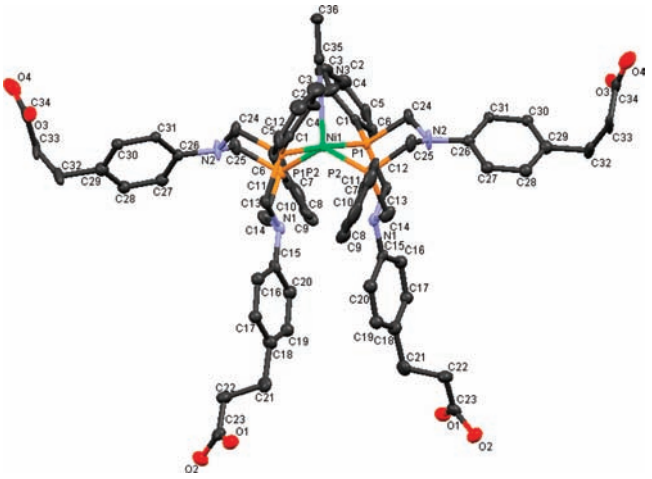

Figure 2. Crystal structure for **4a**. The ellipsoids are drawn at 30% probability, and the hydrogen atoms, counterions, and solvent molecules have been omitted for clarity. Nickel is shown in green, carbon in gray, oxygen in red, nitrogen in purple, and phosphorus in orange.

commonly used in peptide synthesis would be useful, the synthesis of ligand **3d** was achieved by using glycine immobilized on a Wang resin[32] using FMOC chemistry,[23] as shown in reaction (3). The solid-state ^{31}P NMR spectrum of the resin-bound ligand (Figure 1) consists of two resonances at −34.4 and −40.8 ppm. These shifts are downfield of the fully cyclized ligand observed for

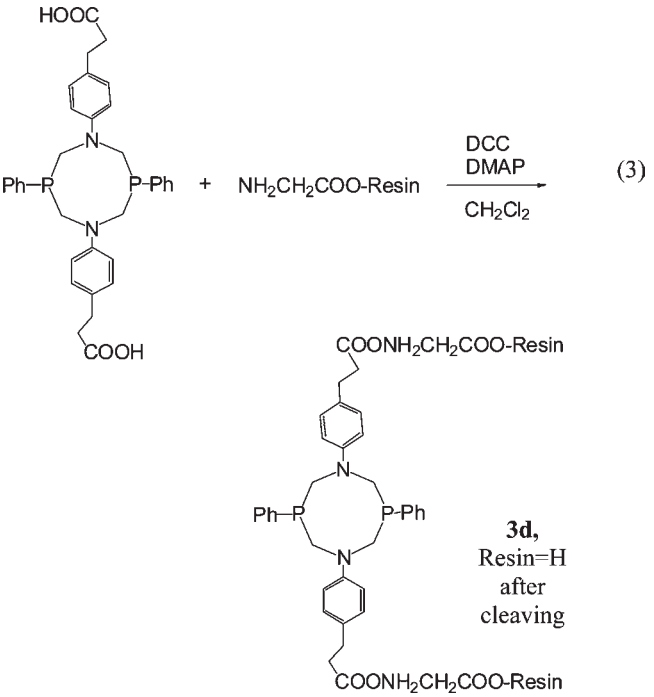

(3)

ligands **3a**−**3c** in solution (−50 ppm) but are consistent with the solid-state NMR of the unbound ligand **3a** (−35.0 ppm, data not shown). The two resonances likely represent isomers of the eight-membered ring, as observed previously for similar soluble ligands prior to metalation.[33−36]

The reaction of stoichiometric amounts of P_2N_2 ligands **3a** and **3b** with $[Ni(CH_3CN)_6](BF_4)_2$ in acetonitrile for 24 h resulted in the formation of red, moderately air-sensitive metal complexes **4a** and **4b**. The crystal structure for **4a** (Figure 2) is very similar to that for $[Ni(P_2{}^{Ph}N_2{}^{Ph})_2(CH_3CN)](BF_4)_2$.[15] Selected bond distances and angles are given in Table 1. The nickel atom is five-coordinate, bound to four phosphorus atoms of two bidentate diphosphine ligands and an acetonitrile molecule, and is best described as distorted trigonal bipyramidal. As with $[Ni(P_2{}^{Ph}N_2{}^{Ph})_2(CH_3CN)](BF_4)_2$, the two nitrogen atoms in the rings in boat conformations are folded toward the nickel center and thus positioned to interact with either a dihydrogen or hydride bound to the nickel, while the other two rings are chair conformations, with the nitrogen atom folded away from the nickel.

Table 1. Selected Bond Distances and Angles for $[Ni(P_2{}^{Ph}N_2{}^{AA})_2(CH_3CN)](BF_4)_2$

Bond Distance (Å)	
Ni1−P1	2.2140(15)
Ni1−P2	2.2179(18)
Ni1−N3	2.003(9)
Ni1---N1	3.393(6)
N3−C35	1.168(13)
Bond Angle (deg)	
P1−Ni1−P2	82.71(6)
P2−Ni1−P2#1	130.35(12)
P1−Ni1−P1#1	175.87(13)
N3−Ni1−P1	92.06(6)
N3−Ni1−P2	114.82(6)
Ni1−N3−C35	180.000(2)

Intermolecular hydrogen bonding is observed between the carboxylic acid groups (Figure 3), with each cation hydrogen bonding to four different cations via the four carboxylic acid groups. Cations connected by hydrogen bonds form planes, which interpenetrate with other hydrogen-bonding planes in the three-dimensional structure. No intramolecular hydrogen bonding was detected.

The $^{31}P\{^1H\}$ and ^1H NMR, cyclic voltammetry, and mass spectrometry data are consistent with the assigned structures of the metal complexes. The $^{31}P\{^1H\}$ NMR of metal complexes **4a** and **4b** in deuteroacetonitrile each displayed a single resonance at 5.3 and 5.0 ppm, respectively (Figure 4), similar to the value reported for $[Ni(P_2{}^{Ph}N_2{}^{Ph})_2(CH_3CN)](BF_4)_2$ (4.82 ppm).[14] At −60 °C in deuteroacetone, two resonances were observed in the ^{31}P NMR spectra for both of these complexes (Figure 4). These resonances are attributed to axial and equatorial phosphorus atoms expected for a five-coordinate trigonal-bipyramidal complex with an equatorial acetonitrile ligand. At room temperature, the rate of exchange of the axial and equatorial phosphorus atoms (Berry pseudorotation) is fast, which averages the ^{31}P NMR resonances, resulting in a single observed resonance. At reduced temperatures, the slowed exchange process results in a static five-coordinate species with resolved chemical shifts. This behavior has been observed previously for analogous metal complexes.[16]

For complex **4c**, a more complex ^{31}P NMR spectrum is observed at room temperature with a broad singlet at 4.04 ppm and two broad resonances at +21.6 and −13.6 ppm at room temperature (Figure 5, left). The central resonance has a chemical shift similar to the exchange-averaged peak seen in the

dx.doi.org/10.1021/ic1025872 |*Inorg. Chem.* 2011, 50, 4073–4085

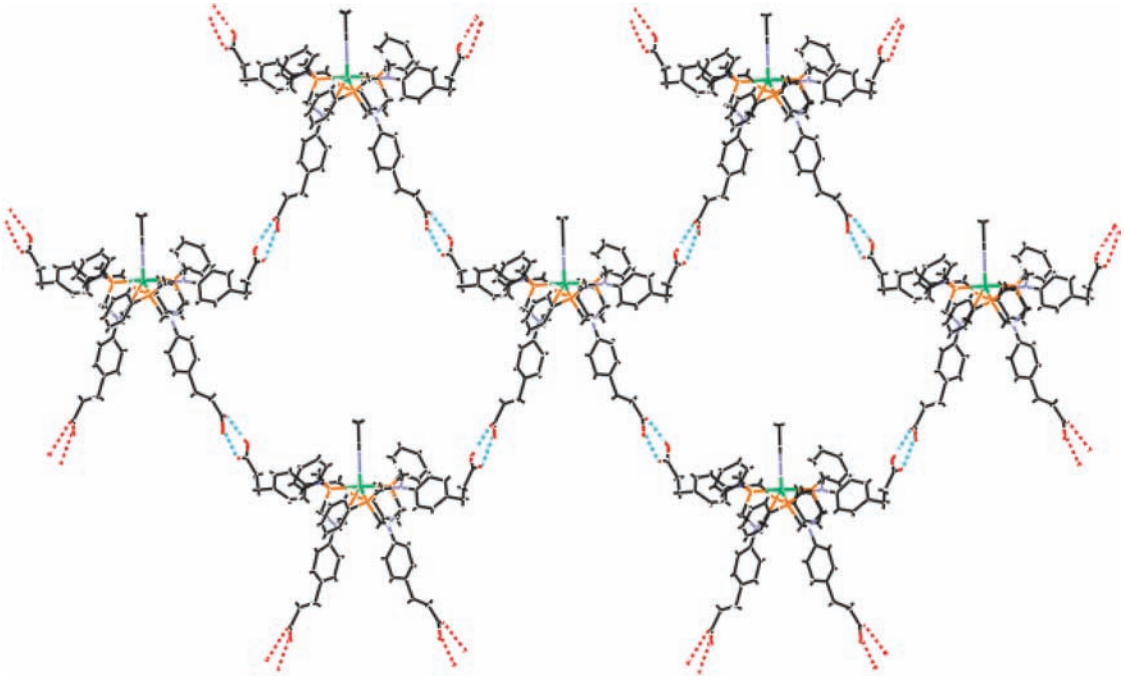

Figure 3. Hydrogen bonding observed for crystals of **4a**. Solvent molecules and anions have been omitted for clarity.

single amino acid modified catalysts **4a** and **4b**. The two additional resonances are symmetric about the central resonance. Upon warming of the NMR solution to 60 °C, the peak at 4.0 ppm became sharper and the peaks at 21.8 and −13.6 ppm broadened. Using acetone as a solvent to extend the low-temperature range, the sample temperature was reduced to −60 °C. At this temperature, the central resonance was unobservable and only the two multiplets at +23.5 and −12.0 ppm were observed. Additionally, ^{31}P−^{31}P EXSY at 20 °C (Figure S1 in the Supporting Information) shows cross peaks between all three resonances, indicating that the sites for the two symmetric resonances are in exchange with the site of the central resonance as well as with each other. This does not distinguish between intra- and intermolecular exchange (both would be observed), but it does confirm that the three sites are able to exchange with each other. Taken together, these data are most consistent with a single complex exhibiting one or more exchange processes. These exchange processes could include restricted Berry pseudorotation or reversible dissociation of a fifth ligand at elevated temperatures and a static structure at low temperature. Although no ^{31}P−^{31}P COSY crosspeaks are observed at either −40 or +30 °C between the central resonance and the symmetric resonances (cross peaks were observed between the two symmetric resonances), this is not surprising because of the lack of resolved splitting.

The variable-temperature NMR data suggest that **4c**, the dipeptide ester ligand, is undergoing exchange processes similar to **4a** and **4b**, the amino acid ligands, but at higher temperatures. This could be due to intra- or intermolecular hydrogen bonding restricting Berry pseudorotation or the fact that the fifth ligand in **4c** is not acetonitrile, as it is for **4a** and **4b**.

In previous studies, we have observed that amides can act as good ligands to these Ni^{2+} complexes. For example, dissolving $[Ni(P^{Ph}{}_2N^{PhCF_3}{}_2)_2](BF_4)_2$ (where $PhCF_3$ is 4-$CF_3C_6H_4$) in dimethylformamide can result in displacement of the diphosphine ligand by dimethylformamide.[37] Because our complexes have amide groups, it is possible that they are binding to the nickel as a fifth ligand, causing the anomalous features in the ^{31}P NMR spectrum. To test this hypothesis, **4b** was titrated with the ethyl ester of the glycylglycine dipeptide and monitored by ^{31}P NMR (Figure 6). Complex **4b** was used to avoid amide or acid functionalities in the metal complex. Because of the limited solubility of the dipeptide in acetonitrile, the experiment was performed in methanol-d_4. The ^{31}P NMR spectrum of complex **4b** displayed a single resonance at 6.2 ppm. Upon an increase in the concentration of the dipeptide, two resonances at +23.2 and −15.2 ppm grew and the central resonance at 6.2 ppm disappeared, demonstrating that the presence of the dipeptide can result in a similar restriction of motion. A similar experiment was performed by adding ethyl acetate; however, in this case, no change was observed in the ^{31}P NMR spectra, suggesting that the ester carbonyl is not involved in the interaction. Modeling studies demonstrated that, because of the rigidity and length of the aromatic ring, neither the amide nor the carbonyl groups within the same molecule are able to interact with the nickel center (Figure 7), so a bimolecular interaction would be required to bind an amide as a fifth ligand.

Another origin of the restricted motion in **4c** could be due to hydrogen bonding. The modeling discussed above indicates that *intra*molecular hydrogen bonding between peptide chains is possible (Figure 7). The crystal structure of **4a** provides evidence that *inter*molecular hydrogen bonding between peptide chains is also possible (Figure 3). Both of these methods provide support for the interpretation that hydrogen bonding between peptide chains could be present in these catalysts. Consequently, two interpretations describing the restricted motion observed by ^{31}P NMR are consistent with the collective data: an amide functional group from a second nickel complex could occupy the fifth-coordination site in **4c**, or intra- or intermolecular hydrogen bonding between peptide chains could result in restricted Berry pseudorotation.

dx.doi.org/10.1021/ic1025872 |*Inorg. Chem.* 2011, 50, 4073–4085

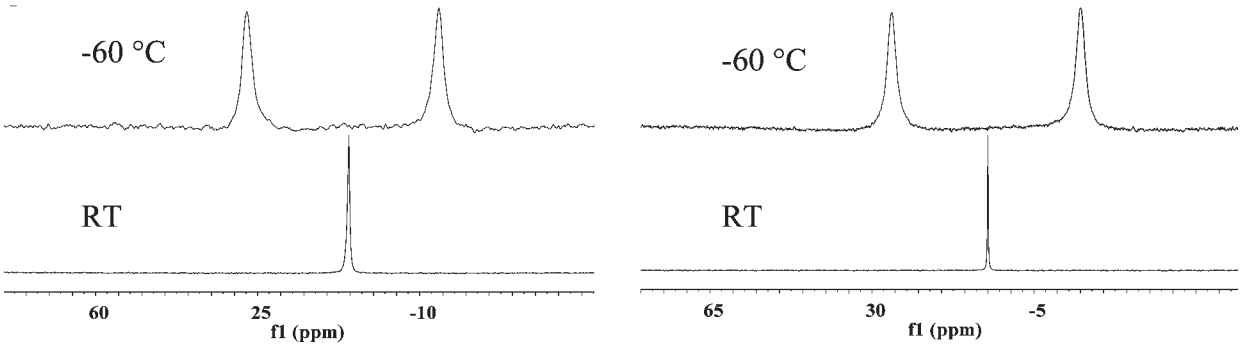

Figure 4. $^{31}P\{^{1}H\}$ NMR spectra of **4a** (left) and **4b** (right) at room temperature (bottom) and −60 °C (top) in acetone-*d*.

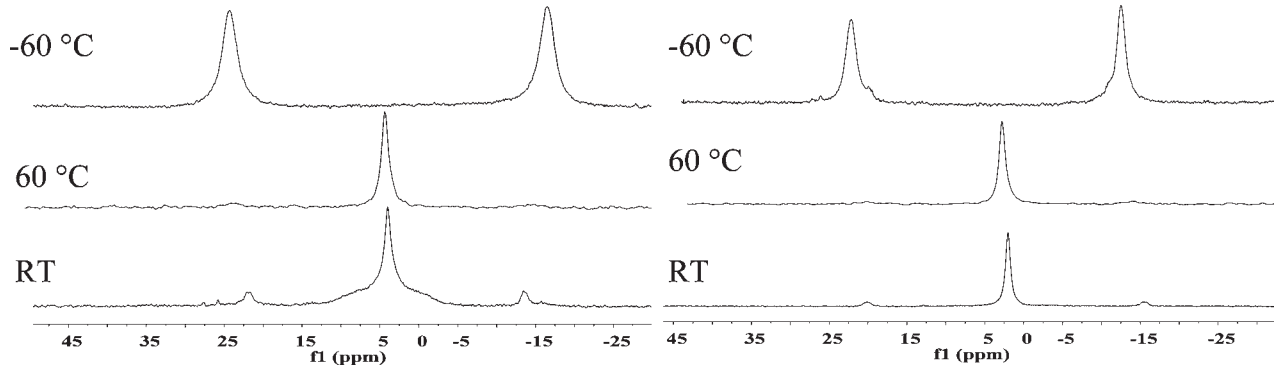

Figure 5. $^{31}P\{^{1}H\}$ NMR spectra of complexes **4c** (left) and **4d** (right) at room temperature (bottom), 60 °C in CD_3CN (middle), and −60 °C (top) in acetone-*d*.

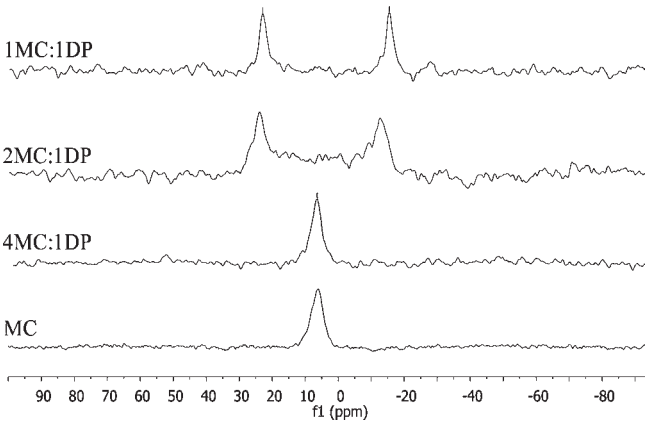

Figure 6. Room temperature $^{31}P\{^{1}H\}$ NMR spectra of complex **4b**, showing the effect of an increase in the concentration of the glycylglycine ethyl ester dipeptide. The ratio of the metal complex to the dipeptide is shown on the left-hand side of the spectra (MC = metal complex; DP = dipeptide glycylglycine ethyl ester).

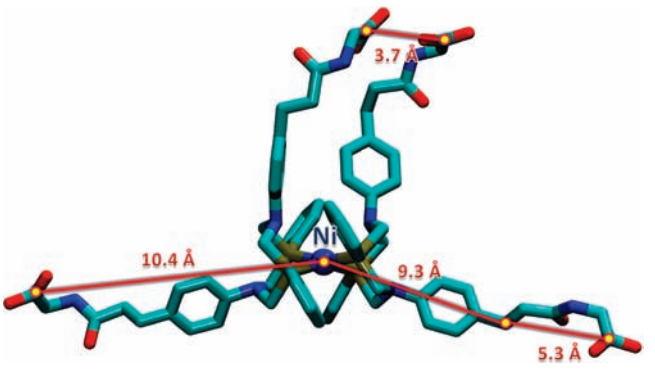

Figure 7. Complex **4d** generated by molecular modeling demonstrates that an intramolecular fifth-coordination site of the amide or carbonyl groups is not possible, but intramolecular hydrogen bonding between peptide chains could occur.

The metal complex **4d** was prepared by adding $[Ni(CH_3CN)_6](BF_4)_2$ to the resin-immobilized ligand. The solid-state NMR spectrum shows nearly complete incorporation of the metal, as demonstrated by the two equivalent downfield resonances (Figure 1, top). Upon cleavage from the resin, the solution-state behavior is very similar to that of **4c**. The $^{31}P\{^{1}H\}$ NMR spectrum of **4d** exhibits a broad singlet at 4.0 ppm at room temperature and two small peaks symmetrically placed about the central resonance at +21.6 and −13.6 ppm (Figure 5). The two symmetrical resonances also become broadened at 60 °C, indicating an exchange process similar to that observed for **4c**.

Electrochemical Studies. Complex **4b** displays two reversible one-electron reductions at −0.83 and −1.04 V versus the ferrocenium/ferrocene couple at a scan rate of 50 mV/s in acetonitrile (Figure 8, left side). These couples are assigned to the $Ni^{II/I}$ and $Ni^{I/0}$ reductions, respectively. The electrochemistry of this complex is consistent with that of the previously reported parent $[Ni(P^{Ph}{}_2N^{Ph}{}_2)_2]^{2+}$ complex.[13,14] The cyclic voltammogram of **4a** displays similar reversible $Ni^{II/I}$ and $Ni^{I/0}$ couples at −0.82 and −1.02 V in benzonitrile. In acetonitrile, two

dx.doi.org/10.1021/ic1025872 |*Inorg. Chem.* 2011, 50, 4073–4085

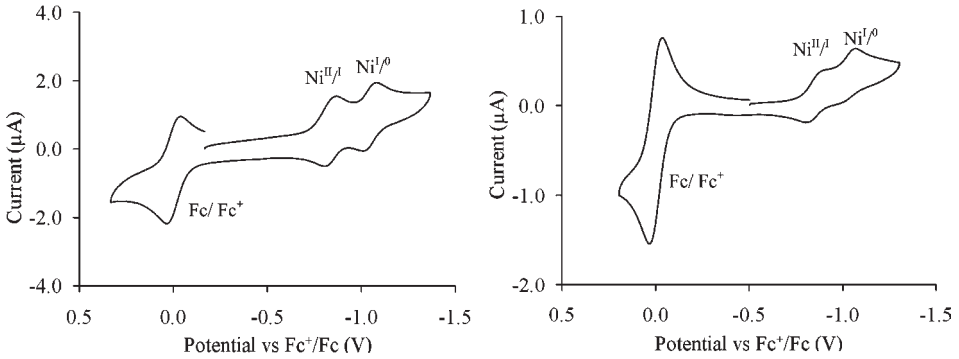

Figure 8. Cyclic voltammograms of 0.65 M solutions of **4b** (left) and **4c** (right) in acetonitrile containing a 0.2 M $^{n}Bu_4N^+OTf^-$ electrolyte using a scan rate of 50 mV/s. Ferrocene was used as an internal standard.

irreversible one-electron waves at −0.82 and −0.98 V are observed corresponding to $Ni^{II/I}$ and $Ni^{I/0}$ reductions, respectively. The irreversibility of the $Ni^{II/I}$ and $Ni^{I/0}$ couples of **4a** can be attributed to the insolubility of the Ni^0 complex in acetonitrile, which precipitates on the electrode surface upon reduction to Ni^0 and retards electron transfer during the oxidative sweep. The cyclic voltammograms of **4c** and **4d** display reversible $Ni^{II/I}$ couples, but in contrast to **4a** and **4b**, quasi-reversible $Ni^{I/0}$ reductions are observed (Figure 8, right side, **4c**).

Catalytic Studies. Figure 9 shows successive cyclic voltammograms of metal complexes **4a**−**4d** recorded in acetonitrile with increasing concentrations of *p*-cyanoanilinium (pK_a 7.0).[38] A catalytic wave for the reduction of protons to dihydrogen is observed with a half-wave potential near the $Ni^{II/I}$ couples of the respective catalysts. At low acid concentrations, the catalytic current increases as the acid concentration increases, until acid concentrations above approximately 0.15 M, where the current is independent of the acid concentration. Repeating selected experiments in the absence of ferrocene yielded identical results.

Plotting the ratio of the observed catalytic current (i_c) to the current of the $Ni^{II/I}$ reduction in the absence of acid (i_p) versus the concentration of acid results in a linear relationship at low acid concentrations (Figure 10 and S2−S4 in the Supporting Information), suggesting that the reaction is second-order in acid (eq 4) below ∼0.04 M *p*-cyanoanilinium.[13,15,17,19]

$$\frac{i_c}{i_p} = \frac{2}{0.4463}\sqrt{\frac{RTk[H^+]^2}{Fv}} \qquad (4)$$

At higher acid concentrations, no acid dependence was observed, consistent with previous dihydrogen production catalysts of this type.[13,14,20] The dependence on the acid concentration has previously been compared to Michaelis−Menten saturation kinetics,[13] where catalysis becomes independent of the substrate under conditions of a large substrate excess (see the Supporting Information, eqs S1−S5). In this region, the rate is equivalent to the release of hydrogen, the rate-limiting step.[16,20] Turnover frequencies were calculated from the acid-independent region using eq 5.[13]

$$\frac{i_c}{i_p} = \frac{2}{0.4463}\sqrt{\frac{RTk}{Fv}} \qquad (5)$$

In this acid-independent region, turnover frequencies of 14, 15, 23, and 25 mol of dihydrogen per 1 mol of catalyst per second are observed for **4a**−**4d**, respectively (Table 2), in the presence of *p*-cyanoanilinium.

Acetonitrile solutions of $DMFH^+$ (pK_a 6.1)[39] gave higher turnover frequencies (450, 140, 1000, and 340 for **4a**−**4d**, respectively) than those obtained with *p*-cyanoanilinium. The turnover frequencies of these complexes are comparable to the turnover frequency for the parent complex $[Ni(P_2^{Ph}N_2^{Ph})_2](BF_4)_2$ measured under similar conditions.[15,16,37] Previous studies have shown that catalytic rates of this class of molecules are first-order in catalyst,[15] and we confirmed this for one of the catalysts in this study (**4a**; see Figure S5 in the Supporting Information).

The overpotential for the catalytic reduction of the protons using *p*-cyanoanilinium was calculated from the half-wave potential of the catalyst and the pK_a value of *p*-cyanoanilinium (7.0)[38] using the method suggested by Evans and co-workers, with $E^\circ_{H+} = -140$ mV.[40] Similar results (within experimental error) were obtained using the method of Fourmond and co-workers.[41] The estimated overpotentials for catalytic reduction of the protons of *p*-cyanoanilinium by **4a**−**4d** are 0.27, 0.27, 0.28, and 0.28 V, respectively (Table 2), and using $DMFH^+$, they are 0.25, 0.25, 0.33, and 0.26 V, respectively. The calculated overpotentials and catalytic rates for peptide-coupled $[Ni(P^R_2N^{R'}_2)_2]^{2+}$ complexes are comparable to the overpotential and catalytic rate of the parent $[Ni(P_2^{Ph}N_2^{Ph})_2]^{2+}$ complex measured under similar conditions.

Electrocatalytic Activity in the Presence of Water. Previous studies in our group suggest an order of magnitude increase in the rates as a function of small amounts of added water using anilinium salts as the acid.[37] The role of water on electrocatalysis of these complexes is intriguing because the fixed proton relay plays such an important role; additional relays, such as closely associated water molecules, may also contribute to efficient proton transfer. The influence of water on the rate of catalysis was determined by recording cyclic voltammograms of metal complexes in acetonitrile in the presence of *p*-cyanoanilinium or $DMFH^+$ and varying the concentrations of water. Large increases in the turnover frequencies were observed upon the addition of water (Figure 11) in the presence of *p*-cyanoanilinium (5−7-fold) compared to $DMFH^+$ (2-fold).

■ DISCUSSION

Enzymes are capable of shuttling gases, protons, and electrons with great speed and precision.[42,43] Enzymes are also capable of very specifically controlling the local environment around the

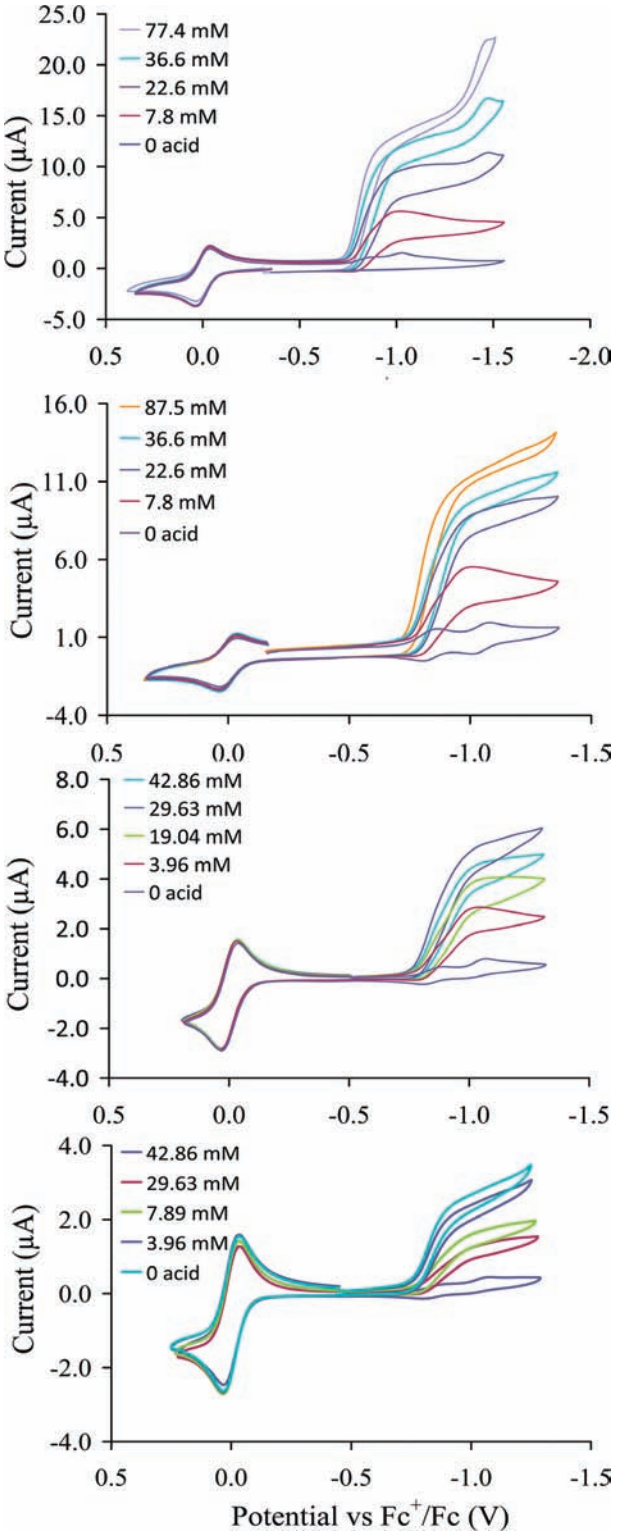

Figure 9. Successive cyclic voltammograms of complexes **4a**−**4d** shown from top to bottom as a function of increasing concentrations of *p*-cyanoanilinium.

active site. Using the large range of functional groups available with the 20 naturally occurring amino acids, and the structural control of the protein architecture, precise placement of hydrophobic or hydrophilic groups can be achieved to control the active-site hydrophobicity, charge, steric accessibility, or electronic character. Furthermore, enzymes are dynamic molecules that can control the desired environment by subtle or significant changes in structure. Like other enzymes, hydrogenase enzymes use many of these outer-coordination-sphere features to very efficiently convert H^+ to H_2 and back again.[1] The $Ni(P_2^RN_2^{R'})_2$ functional mimics of hydrogenase achieve rates that approach those of NiFe hydrogenase but are still an order of magnitude slower than those of FeFe hydrogenase.[15,16] Mimicking the enzymes' placement of a pendant amine in the second-coordination sphere was essential in achieving the current rates.[20] Meeting or exceeding the rates of the enzyme may require mimicking of not only the second-coordination sphere but also the outer-coordination sphere of the enzyme. By building on these active functional hydrogenase mimics, we want to investigate several of these aspects (proton channels, the local environment, and dynamics) of the outer-coordination sphere in a stepwise manner to develop an understanding of their contribution to catalysis, as well as their interdependence upon one another.

Previously, we have attached peptides and polymers to rhodium metal centers to capture the regulatory features of enzymes.[44,45] This effort was aimed at understanding how the reactivity of the metal can be controlled by applying a stimulus to special stimulus-responsive ligands, mimicking the dynamic and regulatory role that outer-coordination spheres of enzymes play. Other groups have also pursued gaining the advantage of some of the features of enzymes.[46−49] Chirality and selectivity[50−56] and active-site pockets[57,58] have been a common focus, but there have been other studies investigating allostery,[50,59] the use of dendrimers for structural and functional control[60,61] and catalyst recovery.[62−64] These approaches often, but not always, utilize amino acids and peptides in their design because of their inherent chirality and the flexibility with the functional group and structural design. More complex approaches have modified existing enzymes[65−69] or designed enzymes de novo,[70,71] both nonmetalated[72−74] and metalated.[75−77] In contrast, our work focuses on the development of new redox-active catalysts that oxidize and produce dihydrogen, utilizing the attributes of the enzyme scaffold as necessary but specifically avoiding reconstruction of the entire enzyme.

The addition of amino acids and small peptides to the $[Ni(P^R_2N^{R'}_2)_2]^{2+}$ catalyst demonstrates two very important advancements in our understanding: (1) Amino acids and peptides can be incorporated into this catalyst core, allowing a foundation for larger peptides that could begin to take advantage of the larger framework used by enzymes, allowing the inclusion of more sophisticated and controlled structures around the active site. (2) The active site is sensitive to very subtle changes far from the active site, suggesting that the outer-coordination sphere can have a large impact on the catalytic rates. In the design of molecular catalysts, it is now well recognized that changes in the first- and second-coordination spheres can have dramatic impacts on catalysis.[20] The results presented in this paper clearly demonstrate that modifications at even greater distances (at least in terms of the number of bonds) can also have significant impacts on the catalytic rates. In this sense, these small molecules are reproducing effects that have been proposed to be important in enzymes.

To build hydrogenase mimics that incorporate features of the outer-coordination sphere, the development of a framework into which peptides can be incorporated was a necessary first step. The current work has demonstrated this capability by utilizing a

dx.doi.org/10.1021/ic1025872 |*Inorg. Chem.* 2011, 50, 4073–4085

Table 2. Turnover Frequencies and Overpotentials of Metal Complexes 4a−4d in Acetonitrile

	turnover frequency (s^{-1}; ±25%; acid, 4-CNAnH$^+$OTf$^-$; electrolyte, ^{n}Bu$_4$N$^+$OTf$^-$)			turnover frequency (s^{-1}; ±10%; acid, DMFH$^+$OTf$^-$; electrolyte, Et$_4$N$^+$BF$_4^-$)		
metal complex	w/o water	w/water ([H$_2$O])	overpotential (V; ±70 mV)	w/o water	w/water ([H$_2$O])	overpotential (V; ±70 mV)
4a	14	71 (0.86 M)	0. 27	450	900 (0.35 M)	0.25
4b	15	62 (0.43 M)	0.27	140	200 (0.50 M)	0.25
4c	23	130 (1.4 M)	0.28	1000	1400 (0.65 M)	0.33
4d	25	180 (1.4 M)	0.28	340	510 (0.50 M)	0.26
[Ni(P$_2^{Ph}$N$_2^{Ph}$)$_2$]$^{2+}$	28	72 (1.1 M)	0.30	590	720 (0.03 M)	0.31

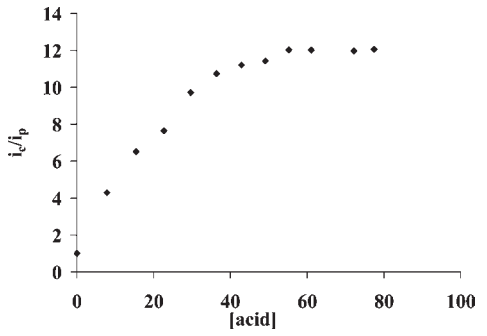

Figure 10. Plot of the ratio of the catalytic current (i_c) to the peak current of the $Ni^{II/I}$ couple in the absence of the acid (i_p) versus the concentration of *p*-cyanoanilinium in acetonitrile. Conditions: 50 mV/s scan rate, 0.2 M ^{n}Bu$_4$N$^+$OTf$^-$/acetonitrile, 0.7 mM complex **4a**, glassy carbon electrode.

non-natural amino acid as a base ligand in the cyclooctane ring [reaction (1)], the carboxylic acid terminus of which allows condensation reactions with other amino acids and peptides. The attachment of additional groups was demonstrated by the addition of a second amino acid [reactions (2) and (3)]. This was achieved using a homogeneous solution-state route in the case of a protected carboxylic acid. However, to attach an unprotected amino acid, solid-phase synthesis (SPS) was required to avoid unwanted side reactions. This also allows easy separation of reactants and products, as has previously been observed when using SPS of organometallic systems.[78] The SPS route provided a clean nickel complex and is the planned synthetic route for the construction of larger peptide-based catalysts. This approach not only avoids the unwanted reaction of the carboxyl terminus but also avoids reactions with functional groups of the side chains, groups that are protected when bound to the resin and deprotected during the cleavage step. Overall, the SPS approach results in a cleanly produced metal complex and eliminates unwanted side reactions.

Importantly, this work demonstrates that the high electrocatalytic activity of the parent complex is maintained in the presence of bulky groups with multiple functionalities (Figure 9 and Table 2), a critical baseline to establish before the attachment of larger peptides. For example, complexes **4a** and **4d** with catalytic rates of 450 and 340 s^{-1}, respectively, are quite comparable to [Ni(P$^{Ph}_2$N$^{Ph}_2$)$_2$]$^{2+}$ with 590 s^{-1}. Similar overpotentials are also observed, indicating that, on the whole, the peptide catalysts behave similarly to the parent complex.

Another similarity between the peptide catalysts and the parent catalyst is the strong dependence on water and on the acid type.[37] For instance, when using *p*-cyanoanilinium as the acid, rates for the peptide catalysts are 14−25 s^{-1}. These rates increase an order of magnitude or more when using DMFH$^+$, where the observed rates are 140−1000 s^{-1}. Catalytic rates are also observed to show significant enhancement (1.4−7 times faster) when water is added to the acidic solution. The difference in rates with different acids has been addressed extensively in a separate paper,[37] and is thought to be related to the substrate size; DMFH$^+$ is a smaller acid than *p*-cyanoanilinium and, consequently, has better access to the crowded area around the protonated amine. The effect of acid pK_a was also investigated[37] and found not to correlate with rate trends in a meaningful way. The argument of the acid size can also explain the increased rates observed in the presence of water. Note that, in the presence of *p*-cyanoanilium, metal complexes display a much larger rate enhancement with added water than in DMFH$^+$. It was proposed that water facilitates the movement of the proton from the exo to the endo position on the amine, the position required for dihydrogen elimination. The effect is more enhanced for *p*-cyanoanilium because its larger size decreases accessibility to the amine, a problem not as pronounced for the smaller DMFH$^+$. Studies are ongoing to further develop the mechanism explaining the catalytic impact that the acid size and water have on catalysis.

While the catalysts are similar to the parent complex, there are clear effects of the outer-coordination sphere, even with the relatively simple modifications introduced by the mono- and dipeptides. Of note is that **4c** is one of the fastest reported catalysts of this type using DMFH$^+$, in both the presence and absence of water.[37] At the same time, there are trends that are difficult to explain. Electrocatalysis using *p*-cyanoanilinium as the acid shows that the peptide catalysts have rates (∼0.5−1 times) similar to that of the parent phenyl-substituted complex (Table 2) in the absence of water and the rates increase with increasing peptide size. However, the electrochemistry of the same catalysts using DMFH$^+$ as the acid shows no clear correlation between the ligand size (one or two amino acids) or the functional group (acid or ester termination). Under these conditions, the peptides range from ∼2 times faster (**4d**) than the parent complex to ∼4 times slower (**4b**). The larger size due to incorporation of a glycine unit for the two ester-terminated catalysts **4b** and **4c** results in a 4−8-fold increase in the rate. This is a surprising increase for a relatively simple modification and is not observed for the corresponding acid-terminated catalysts **4a** and **4d**, which have rates very similar to each other and demonstrate the opposite trend with respect to the additional glycine unit; i.e., **4d** is slightly slower than **4a** when compared to the ester derivatives.

dx.doi.org/10.1021/ic1025872 |*Inorg. Chem.* 2011, 50, 4073–4085

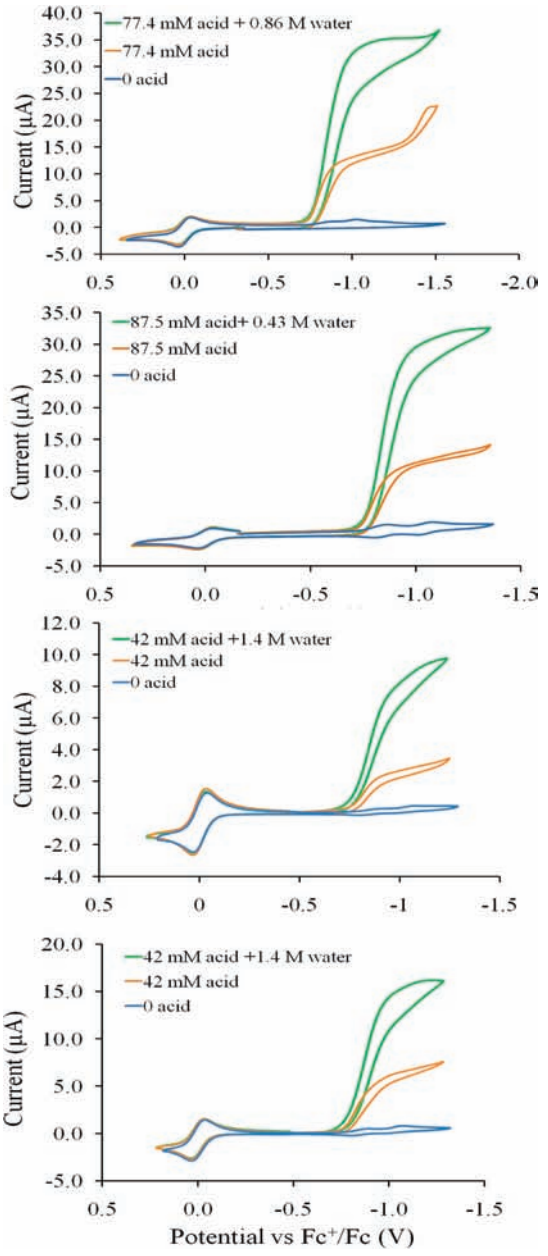

Figure 11. Cyclic voltammograms of **4a**−**4d** in the presence of *p*-cyanoanilinium (orange trace) and water (green trace).

Restricted motional processes for the dipeptide metal complexes, **4c** and **4d**, appear to arise from intermolecular interactions of the dipeptide functional groups. However, the observed restricted motion does not appear to be correlated with electrocatalysis. For instance, **4c** and **4d** both exhibit the ^{31}P NMR spectrum, indicating restricted motion; however, one is faster and one slower than the single amino acid analogues, where restricted motion is not observed. It is likely that, as the outer-coordination sphere includes more complex side chains (polar, charged, acidic, and basic) and gets larger, additional interactions will be observed and the development of a mechanism will be possible. Even within the limited set of data presented in this manuscript, it is clear that apparently subtle changes in the outer-coordination sphere can significantly modulate the catalytic activity.

SUMMARY

In order to more fully understand the contribution of the outer-coordination sphere to the catalytic activity of hydrogenase enzymes, functional mimics containing short peptides in the outer-coordination sphere have been synthesized, characterized, and studied. Mono- and dipeptides were introduced to a previously reported complex $[Ni(P_2^{Ph}N_2^{Ph})_2]^{2+}$, which has been shown to display a high catalytic rate (590−720 s^{-1}) and a moderate overpotential (310 mV) using $DMFH^+$ as the acid. These peptide-containing complexes are moderately air-stable and can be prepared in good yields. All four complexes are active catalysts for the reduction of protons to dihydrogen, ranging from ∼4 times slower to ∼2 times faster than the parent catalyst. The observed differences in the catalytic rates for these complexes with the introduction of minor modifications in the outer-coordination sphere indicate that the outer-coordination sphere can significantly enhance or decrease the rate of catalysis compared to the parent complex. Of particular note, complex **4c** exhibits rates 4−8 times that of **4b**, which differ only by the presence of a glycine unit, with a dramatic change in rate resulting from a small structural change. In addition, the introduction of short peptides in the nickel-based hydrogen production electrocatalysts establishes a framework for extension of this work to larger peptides to more closely mimic enzyme structures.

ASSOCIATED CONTENT

Supporting Information. ^{31}P−^{31}P EXSY data, plots of i_c/i_p versus acid concentration for **4b**−**4d**, derivation of Michaelis−Menten kinetics, linear dependence on the catalyst concentration, and a CIF file for the crystal structure of **4a**. This material is available free of charge via the Internet at http://pubs.acs.org.

AUTHOR INFORMATION

Corresponding Author
*E-mail: wendy.shaw@pnl.gov.

ACKNOWLEDGMENT

We thank Dr. John Roberts for useful discussion. This work was supported by the U.S. Department of Energy Basic Energy Sciences, Chemical Sciences, Geosciences & Biosciences Division. The Pacific Northwest National Laboratory is operated by Battelle for the U.S. Department of Energy.

REFERENCES

(1) Fontecilla-Camps, J. C.; Volbeda, A.; Cavazza, C.; Nicolet, Y. *Chem. Rev.* **2007**, *107*, 4273–4303.
(2) Frey, M. *ChemBioChem* **2002**, *3*, 153–160.
(3) Nicolet, Y.; de Lacey, A. L.; Vernede, X.; Fernandez, V. M.; Hatchikian, E. C.; Fontecilla-Camps, J. C. *J. Am. Chem. Soc.* **2001**, *123*, 1596–1601.
(4) Peters, J. W.; Lanzilotta, W. N.; Lemon, B. J.; Seefeldt, L. C. *Science* **1998**, *282*, 1853–1858.
(5) Shima, S.; Pilak, O.; Vogt, S.; Schick, M.; Stagni, M. S.; Meyer-Klaucke, W.; Warkentin, W.; Thauer, R. K.; Ermler, U. *Science* **2008**, *321*, 572–575.
(6) Volbeda, A.; Charon, M.-H.; Piras, C.; Hatchikian, E. C.; Frey, M.; Fontecilla-Camps, J. C. *Nature* **1995**, *373*, 580–587.
(7) Volbeda, A.; Garcin, E.; Piras, C.; de Lacey, A. L.; Fernandez, V. M.; Hatchikian, E. C.; Frey, M.; Fontecilla-Camps, J. C. *J. Am. Chem. Soc.* **1996**, *118*, 12989–12996.

(8) Gloaguen, F.; Rauchfuss, T. B. *Chem. Soc. Rev.* **2009**, *38*, 100–108.
(9) Henry, R. M.; Shoemaker, R. K.; DuBois, D. L.; Rakowski DuBois, M. *J. Am. Chem. Soc.* **2006**, *128*, 3002–3010.
(10) Henry, R. M.; Shoemaker, R. K.; Newell, R. H.; Jacobsen, G. M.; DuBois, D. L.; Rakowski DuBois, M. *Organometallics* **2005**, *24*, 2481–2491.
(11) Jacobsen, G. M.; Shoemaker, R. K.; McNevin, M. J.; Rakowski DuBois, M.; DuBois, D. L. *Organometallics* **2007**, *26*, 5003–5009.
(12) Jacobsen, G. M.; Yang, J. Y.; Twamley, B.; Wilson, A. D.; Bullock, M.; Rakowski DuBois, M.; DuBois, D. L. *Energy Environ. Sci.* **2008**, *1*, 167–174.
(13) Pool, D. H.; DuBois, D. L. *J. Organomet. Chem.* **2009**, *694*, 2858–2865.
(14) Wilson, A. D.; Fraze, K.; Twamley, B.; Miller, S. M.; DuBois, D. L.; Rakowski DuBois, M. *J. Am. Chem. Soc.* **2008**, *130*, 1061–1068.
(15) Wilson, A. D.; Newell, R. H.; McNevin, M. J.; Muckerman, J. T.; Rakowski DuBois, M.; DuBois, D. L. *J. Am. Chem. Soc.* **2006**, *128*, 358–366.
(16) Wilson, A. D.; Shoemaker, R. K.; Miedaner, A.; Muckerman, J. T.; DuBois, D. L.; DuBois, M. R. *Proc. Natl. Acad. Sci. U.S.A.* **2007**, *104*, 6951–6956.
(17) Yang, J. Y.; Bullock, R. M.; Shaw, W. J.; Twamley, B.; Fraze, K.; Rakowski DuBois, M.; DuBois, D. L. *J. Am. Chem. Soc.* **2009**, *131*, 5935–5945.
(18) Curtis, C. J.; Miedaner, A.; Ciancanelli, R.; Ellis, W. W.; Noll, B. C.; Rakowski DuBois, M.; DuBois, D. L. *Inorg. Chem.* **2003**, *42*, 216–227.
(19) Fraze, K.; Wilson, A. D.; Appel, A. M.; Rakowski DuBois, M.; DuBois, D. L. *Organometallics* **2007**, *26*, 3918–3924.
(20) Rakowski DuBois, M.; DuBois, D. L. *Chem. Soc. Rev.* **2009**, *38*, 62–72.
(21) Leger, C.; Jones, A. K.; Roseboom, W.; Albracht, S. P. J.; Armstrong, F. A. *Biochemistry* **2002**, *41*, 15736–15746.
(22) Le Goff, A.; Artero, V.; Jousselme, B.; Tran, p. D.; Guiller, N.; Metaye, R.; Fihri, A.; Palacin, S.; Fontecave, M. *Science* **2009**, *326*, 1384–1387.
(23) Meienhofer, J.; Waki, M.; Heimer, E. P.; Lambros, T. J.; Makofske, R. C.; Chang, C.-D. *J. Pept. Protein Res.* **19779**, No. 13, 35–42.
(24) *Brüker APEX 2*, version 2010.3-0; Brüker AXS Inc.: Madison, WI, 2009.
(25) *SAINTPlus: Data Reduction and Correction Program*, version 723a; Bruker AXS Inc.: Madison, WI, 2004.
(26) *SADABS: an Empirical Absorption Correction Program*, version 2001/1; Bruker AXS Inc.: Madison, WI, 2001.
(27) Sheldrick, G. M. *SHELXTL: Structure Determination Software Suite*, version 6.14; Bruker AXS Inc.: Madison, WI, 2004.
(28) Stewart, J. *J. Mol. Model.* **2007**, *13*, 1173–1213.
(29) Correa, A.; Ragone, F.; Cavallo, L. *Green metathesis chemistry: great challenges in synthesis, catalysis and nanotechnology*; Springer: Amsterdam, The Netherlands, 2010.
(30) Sorkin, D.; Truhlar, G.; Amin, E. A. *J. Chem. Theory Comput.* **2009**, *5*, 1254–1265.
(31) Vande Vondele, J. K. M.; Mohamed, F.; Parrinello, M.; Chassaing, T.; Hutter, J. *Comput. Phys. Commun.* **2005**, *167*, 103.
(32) Wang, S.-S. *J. Am. Chem. Soc.* **1973**, *95*, 1328–1333.
(33) Weidner, E.; Yang, J. Y.; Dougherty, W. G.; Kassel, W. S.; Bullock, R. M.; Rakowski DuBois, M.; DuBois, D. L. *Organometallics* **2010**, *29*, 5390–5401.
(34) Albrand, J. P. G. D.; Robert, J. B. *Chem. Commun.* **1968**, 1469–1470.
(35) Albrand, J. P. G. D.; Picard, M.; Robert, J. B. *Tetrahedron Lett.* **1970**, *11*, 4593–4596.
(36) Märkl, V. G. J. G. Y.; Schoerner, C. *Tetrahedron Lett.* **1980**, *21*, 1409–1412.
(37) Kilgore, U. J.; Roberts, J. A. S.; Pool, D. H.; Appel, A. M.; Stewart, M. P.; Rakowski DuBois, M.; Dougherty, W. G.; Kassel, W. S.; Bullock, R. M.; DuBois, D. L. *J. Am. Chem. Soc.* **2011**, No. 133, XX, accepted for publication.
(38) Appel, A. M.; Lee, S.-J.; Franz, J. A.; DuBois, D. L.; Rakowski DuBois, M.; Twamley, B. *Organometallics* **2009**, *28*, 749–754.
(39) Izutsu, K. *Acid—Base Dissociation Constants in Dipolar Aprotic Solvents*; Blackwell Scientific Publications: Oxford, U.K., 1990.
(40) Felton, G. A. N.; Glass, R. S.; Lichtenberger, D. L.; Evans, D. H. *Inorg. Chem.* **2006**, *45*, 9181–9184.
(41) Fourmond, V.; Jacques, P.-A.; Fontecave, M.; Artero, V. *Inorg. Chem.* **2010**, *49*, 10338–10347.
(42) Creighton, T. E. *Proteins*; W. H. Freeman and Company: New York, 1996.
(43) Ragsdale, S. W. *Chem. Rev.* **2006**, *106*, 3317–3337.
(44) Shaw, W. J.; Chen, Y.; Fulton, J.; Linehan, J.; Gutowska, A.; Bitterwolf, T. *J. Organomet. Chem.* **2008**, *693*, 2111–2118.
(45) Shaw, W. J.; Linehan, J. C.; Gutowska, A.; Newell, D.; Bitterwolf, T.; Fulton, J. L.; Chen, Y.; Windisch, C. F. *Inorg. Chem. Commun.* **2005**, *8*, 894–896.
(46) Loganson, A. A. *Russ. Chem. Rev.* **1985**, *54*, 277–292.
(47) Wohrle, D. *Angew. Chem., Int. Ed.* **2005**, *44*, 7500–7502.
(48) Severin, K.; Bergs, R.; Beck, W. *Angew. Chem., Int. Ed.* **1998**, *37*, 1634–1654.
(49) Ogawa, M. Y.; Gretchikhine, A. B.; Soni, S.-D.; Davis, S. M. *Inorg. Chem.* **1995**, *34*, 6423–6424.
(50) Gianneschi, N. C.; Bertin, P. A.; Nguyen, S. T.; Mirkin, C. A.; Zakharov, L. N.; Rheingold, A. L. *J. Am. Chem. Soc.* **2003**, *125*, 10508–10509.
(51) Knor, G. *ChemBioChem* **2001**, *7/8*, 593–596.
(52) Breit, B.; Seiche, W. *Angew. Chem., Int. Ed.* **2005**, *44*, 1640–1643.
(53) Lordi, V.; Yao, N.; Wei, J. *Chem. Mater.* **2001**, *13*, 733–737.
(54) Miller, S. J. *Acc. Chem. Res.* **2004**, *37*, 601–610.
(55) Roelfes, G.; Feringa, B. L. *Angew. Chem., Int. Ed.* **2005**, *44*, 3230–3232.
(56) Erickson, L. E.; Bailey, P. D.; Kimball, T. L.; Morgan, B. R. *Inorg. Chim. Acta* **2003**, *346*, 169–180.
(57) Slagt, V. F.; Reek, J. N. H.; Kamer, P. C. J.; Leeuwen, P. W. N. M. V. *Angew. Chem., Int. Ed.* **2001**, *40*, 4271–4274.
(58) Kersting, B. *Z. Anorg. Allg. Chem.* **2004**, *630*, 765–780.
(59) Berg, T. *Angew. Chem., Int. Ed.* **2009**, *28*, 2–5.
(60) Liang, C.; Frechet, J. M. J. *Prog. Polym. Sci.* **2005**, *30*, 385–402.
(61) Scott, R. W. J.; Datye, A. K.; Crooks, R. M. *J. Am. Chem. Soc.* **2003**, *125*, 3708–3709.
(62) Bergbreiter, D. E. *Chem. Rev.* **2002**, *102*, 3345–3384.
(63) Dickerson, T. J.; Reed, N. N.; Janda, K. D. *Chem. Rev.* **2002**, *102*, 3325–3344.
(64) Madhavan, N.; Jones, C. W.; Weck, M. *Acc. Chem. Res.* **2008**, *41*, 1153–1165.
(65) Nakajima, H.; Ichikawa, Y.; Satake, Y.; Takatani, N.; Manna, S. K.; Rajbongshi, J.; Mazumdar, S.; Watanabe, Y. *ChemBioChem* **2008**, *9*, 2954–2957.
(66) Park, H.-S.; Nam, S.-H.; Lee, J. K.; Yoon, C. N.; Mannervik, B.; Benkovic, S. J.; Kim, H.-S. *Science* **2006**, *311*, 535–538.
(67) Qi, D.; Tann, C.-M.; Haring, D.; Distefano, M. D. *Chem. Rev.* **2001**, *101*, 3081–3111.
(68) Thomas, C. M.; Ward, T. R. *Chem. Soc. Rev.* **2005**, *34*, 337–346.
(69) Walter, K. U.; Vamvaca, K.; Hilvert, D. *J. Biol. Chem.* **2005**, *280*, 37742–37746.
(70) Nanda, V.; Koder, R. L. *Nat. Chem.* **2010**, *2*, 15–24.
(71) Lu, Y.; Yeung, N.; Sieracki, N.; Marshall, N. M. *Nature* **2009**, *460*, 855–862.
(72) Jiang, L.; Althoff, E. A.; Clemente, F. R.; Doyle, L.; Rothlisberger, D.; Zahghellini, A.; Gallaher, J. L.; Betker, J. L.; Tanaka, F.; Barbas, C. F., III; Hilvert, D.; Houk, K. N.; Stoddard, B. L.; Baker, D. *Science* **2008**, *319*, 1387–1391.
(73) Rothlisberger, D.; Khersonsky, O.; Wollacott, A. M.; Jiang, L.; DeChancie, J.; Betker, J.; Gallaher, J. L.; Althoff, E. A.; Zanghellini, A.; Dym, O.; Albeck, S.; Houk, K. N.; Tawfik, D. S.; Baker, D. *Nature* **2008**, *453*, 190–197.
(74) Dwyer, M. A.; Looger, L. L.; Hellinga, H. W. *Science* **2004**, *304*, 1967–1971.

(75) Kaplan, J.; DeGrado, W. F. *Proc. Natl. Acad. Sci. U.S.A.* **2004**, *101*, 11566–11570.
(76) Ghadiri, M. R.; Soares, C.; Choi, C. *J. Am. Chem. Soc.* **1992**, *114*, 4000–4002.
(77) Salgado, E. N.; Radford, R. J.; Tezcan, F. A. *Acc. Chem. Res.* **2010**, *43*, 661–672.
(78) Heinze, K.; Beckmann, M.; Hempel, L. *Chem.—Eur. J.* **2008**, *14*, 9468–9480.